

Bending instabilities at the origin of persistent warps: A new constraint on dark matter halos

Y. Revaz and D. Pfenniger

Geneva Observatory, University of Geneva, 1290 Sauverny, Switzerland
e-mail: Yves.Revaz@obs.unige.ch

Received 29 March 2004 / Accepted 2 June 2004

Abstract. A substantial fraction of the warps in spiral galaxies may result from bending instabilities if the disks are essentially self-gravitating. With N -body simulations, we show that galaxies with self-gravitating disks as thick as HI disks are subject to bending instabilities generating S-shaped, U-shaped or asymmetric warps. S-shaped warps persist during several rotations and keep the line of node straight. The warp amplitudes generated by bending instabilities remain however modest. Other factors must be invoked for extreme warped disks. However, bending instabilities can account for most of the cases reported in optical surveys, where the warp angle is generally less than 5° . This mode of warping is very sensitive to the disk flattening. It also constrains the fraction of dark matter distributed in the disk and in the dark halo.

Key words. galaxies: kinematics and dynamics – methods: N-body simulations – cosmology: dark matter

1. Introduction

Since the first observation of the Milky Way warp at the end of the fifties (Kerr et al. 1956; Burke 1957), half a century has passed without a clear explanation of this feature (see Binney 1992, for a review). The warp problematic comes essentially from its high frequency in spirals. In the local group, including the Milky Way, the three dominant spirals are warped (Roberts 1966; Rogstad et al. 1976; Newton & Emerson 1977) and among nearby galaxies they are common (Sancisi 1976; Bosma 1981). Statistics of warps in HI (Bosma 1991; Richter & Sancisi 1994; García-Ruiz et al. 1998) and in the optical band (Reshetnikov 1998; Reshetnikov & Combes 1999; Sánchez-Saavedra et al. 1990, 2003) reveal that more than half the spiral galaxies are warped and asymmetric. This implies that warps are either frequently or continuously generated, or persistent over several dynamical times. Disks are easily warped when subject to an external torque, generated for example by gravitational forces during interactions (Quinn 1991; Hernquist 1991; Huang & Carlberg 1997) or accretion events (Jiang & Binney 1999; Revaz & Pfenniger 2001b; López-Corredoira et al. 2002), or by magnetic forces in the gas (Battaner et al. 1990). The challenge is to understand how isolated galaxies (in appearance) can conserve their warp with a relatively straight line of nodes (LON), avoiding the winding problem early noticed by Kahn & Woltjer (1959). Solutions like normal modes of vibration (bending waves) have been proposed (Lynden-Bell 1965). Unfortunately Hunter & Toomre (1969) showed that no discrete modes exist in disks with soft edges. If, in the presence of a dark halo, discrete modes can exist (Sparke 1984; Sparke & Casertano 1988) they will be

quickly damped by dynamical friction (Nelson & Tremaine 1995; Dubinski & Kuijken 1995).

However, as pointed out by Sellwood (1996), previous studies have treated the case of a cold razor-thin disk. When taking into account the velocity dispersions necessary to keep the disks stable against axisymmetric instability, disks may be subject to a bending instability (also named fire-hose instability). Bending instabilities were first studied by Toomre (1966) in an infinite slab of finite thickness. The instability occurs when the centrifugal force of particles following a bend in the slab is higher than the gravitational restoring force of the slab itself. A formal description of the instability can be found in Fridman & Polyachenko (1984, p. 37). Araki (1985) showed that an infinite slab is stable when the ratio of the vertical velocity dispersion σ_z to the velocity dispersion in the plane σ_u exceeds 0.293. Sellwood & Merritt (1994) and Merritt & Sellwood (1994) have studied this instability in realistic disks of counter-rotating stellar components. They found discrete bending modes $m = 0$ and $m = 1$ that could persist in disks even without counter-rotation. Sellwood (1996) studied the growth of such modes in axisymmetric cases and found that they are strongly Landau damped (Fridman & Polyachenko 1984). He also mentioned that some warm disks support long-lived axisymmetric flapping oscillations.

Since the end of the sixties, most of the works on the warp problem have been built on the assumption of a disk embedded in a massive non-rotating dark halo. However, there are now many observations that let us think that a substantial fraction of dark matter may be present in outer galactic disks, in the form of rotationally supported cold and clumpy gas (Pfenniger et al. 1994; Pfenniger & Combes 1994).

The presence of a weak but existing star formation rate far from the center of galaxies has been reported by different authors (Naeslund & Joersaeter 1997; Smith et al. 2000; Cuillandre et al. 2001). This star formation rate reveals that molecular gas must be present in abundance in the outer disk of galaxies. Moreover, it has been pointed out long ago by Bosma (1978, 1981) that in samples of galaxies, the ratio between the dark matter and HI surface density is roughly constant well beyond the optical disk (see also Carignan et al. 1990; Broeils 1992; Hoekstra et al. 2001). These observations suggest that the dark matter follows the HI distribution along the disk. More recently, the study of the spiral pattern of NGC 2915 has suggested that the very extended HI disk in this galaxy is supported by a quasi self-gravitating disk (Bureau et al. 1999; Masset & Bureau 2003).

In the context of the warps, massive disks are interesting because the kinetic pressure support is then lower than the rotational support and such disks are in a regime where the Araki criterion (Araki 1985) is relevant, thus bending instabilities are expected.

In the first part, we examine the evolution of bending instabilities in different self-consistent galactic models, where the mass is dominated by a heavy disk. The models differ essentially in the thickness of the heavy disk. We show that between the very unstable thin disks and the stable thick disks, a regime exists where bending instabilities spontaneously generate persistent warps. In the second part, a semi-analytic analysis allows us to fix constraints on the validity of the previous results, when a dark halo is also taken into account. The values of the mass and flattening of the dark halo compatible with bending instabilities is determined.

2. The galaxy model

Our galactic mass model is composed of a bulge, an exponential stellar disk and a heavy disk made of HI gas and dark matter proportional to it.

1. The bulge density profile is a flattened Plummer model:

$$\rho_b(R, z) \propto \left(1 + \frac{R^2}{a^2} + \frac{z^2}{b^2}\right)^{-5/2}, \quad (1)$$

where $a = 1$ kpc and $b = 0.25$ kpc.

2. The exponential stellar disk takes the usual form:

$$\rho_d(R, z) \propto e^{-R/H_R} e^{-|z|/H_z}, \quad (2)$$

where the radial and vertical scale length are respectively $H_R = 2.5$ and $H_z = 0.25$ kpc.

3. To comply with the HI observations and slowly varying rotation curves, the heavy disk density profile is:

$$\rho_{hd}(R, z) \propto \frac{e^{-R/R_{hd}}}{R} \frac{e^{-|z|/h_z(R)}}{h_z(R)} \arccos\left(R/R_{hd}^{\max}\right). \quad (3)$$

For $R > R_{hd} = 7$ kpc, the heavy disk surface density decreases as R^{-1} . It is smoothly truncated by the arccosine function at $R_{hd}^{\max} = 35$ kpc in order to keep an approximately constant rotation curve up to the disk edge. In agreement

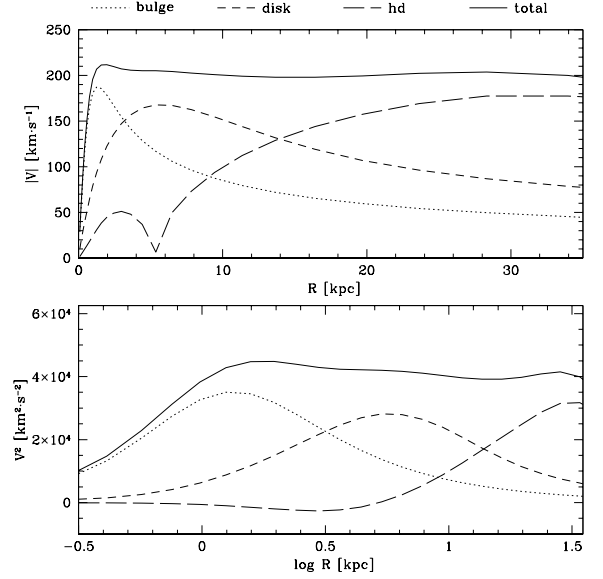


Fig. 1. Contribution of each component to the total rotation curve. The upper panel shows a classical representation of the rotation curve. In the bottom panel, the square of the circular velocity is plotted as a function of $\log R$. The latter representation enhances the effective contribution of each component to the total rotation curve (Kalnajs 1999).

with observations showing that dark matter is not dominant at the center of galaxies (Weiner et al. 2001; Bissantz et al. 2003), the heavy disk surface density drops to zero at the center if $R_{hd} > 0$. To be consistent with the observed flaring of HI in the Milky Way (Burton 1992), the vertical scale height $h_z(R)$ is radius dependent and is written as:

$$h_z(R) = h_{z0} e^{R/R_f}, \quad (4)$$

where h_{z0} is the vertical scale height at the center and R_f the flaring radial scale-length.

The respective masses of the three components are $M_b = 0.15 \times 10^{11} M_\odot$ for the bulge, $M_d = 0.46 \times 10^{11} M_\odot$ for the exponential stellar disk, and $M_{hd} = 1.61 \times 10^{11} M_\odot$ for the heavy disk. With these values the rotation curve is approximately flat up to $R = 35$ kpc. Figure 1 shows the contribution of each component to the total rotation curve. The lack of HI or dark matter at the center of the galaxy implies a negative circular velocity squared contribution by the heavy disk component (see the bottom panel of Fig. 1). In the upper panel, where the norm of the circular velocity is traced as a function of radius, it produces a bump around 3 kpc.

The initial vertical velocity dispersion σ_z is found by satisfying the equilibrium solution of the stellar hydrodynamic equation in cylindrical coordinates (see e.g., Binney & Tremaine 1987, p. 199) separately for each of the bulge, stellar disk and heavy disk components,

$$\rho_i \sigma_{zi}^2 = \int_z^\infty dz \rho_i \partial_z \Phi, \quad (5)$$

where the index i can label any component. These calculations are carried out on the polar coordinate potential solver of the Particle-Mesh N -body code described in

Pfenniger & Friedli (1993). The ratio between the tangential velocity dispersion σ_ϕ and the radial one σ_R is derived from the epicycle approximation (Binney & Tremaine 1987, p. 125):

$$\frac{\sigma_\phi^2}{\sigma_R^2} = \frac{\kappa^2}{4\Omega^2} = \frac{R^{-3}\partial_R(R^3\partial_R\Phi)_{z=0}}{4R^{-1}(\partial_R\Phi)_{z=0}}, \quad (6)$$

where κ is the radial epicyclic frequency, and Ω the rotation frequency, determined from the potential R -derivatives as indicated in Eq. (6). Since in this approximation the radial oscillations are decoupled from the vertical oscillations, the ratio σ_z/σ_R , which is precisely the Araki criterion, is not constrained. This allows us to choose the radial velocity dispersion. We have used the following relation:

$$\frac{\sigma_z^2}{\sigma_R^2} = \beta^2 \frac{\kappa^2}{\nu^2} = \beta^2 \frac{R^{-3}\partial_R(R^3\partial_R\Phi)_{z=0}}{(\partial_z^2\Phi)_{z=0}}, \quad (7)$$

where ν is the vertical epicycle frequency, determined from the potential z -derivatives as indicated in Eq. (7). The factor β is constant of order 1 and chosen to fix the Sæveron-Toomre radial stability parameter $Q = \kappa\sigma_R/3.36G\Sigma$, where $\Sigma = 2\int_0^\infty dz\rho(R,z)$ is the total surface density.

The found velocity dispersions are then used to distribute the model particles in velocity space and to find the rotation velocity for each component with the Jeans equations.

3. The simulations

3.1. Parameters

In order to explore the existence and evolution of bending instabilities, we have run a set of 9 models that differ in the thickness of the heavy disk, parameterized by R_f and h_{z0} . Values are chosen such that the minimal ratio σ_z/σ_R in the disk ranges in an interval around Araki's limit¹. At equilibrium, σ_z^2 is proportional to the thickness of the disk. From Eq. (7), the ratio σ_z/σ_R strongly depends on the second z -derivative of the potential. Thus, increasing the thickness of the disk increases the ratio σ_z/σ_R . Moreover, since σ_z and σ_R are linked by Eq. (7) and since κ and the surface density Σ are almost independent of the vertical thickness, thinner disks are also more unstable with respect to the radial stability parameter Q . In Fig. 2, for each model, Q and σ_z/σ_R are traced as functions of the radius. With the parameter β fixed to 0.77, all models are slightly sub-critical with respect to the generation of spiral density waves.

Figure 3 shows the distribution of the models in the plane σ_z - σ_z/σ_R , at the radius R where σ_z/σ_R is minimal. Thin disks are found at lower left end while thick disks are found at the upper right end. The dotted line corresponds to Araki's limit. Parameters for each model, as well as $(\sigma_z/\sigma_R)_{\min}$ and the flattening ζ of the potential are summarized in Table 1. The potential flattening is defined as the ratio of minor over major axis of the iso-potentials.

¹ Araki's criterion has been derived in the case of an infinite slab. However, it remains locally a good first order approximation when the rotation support exceeds the radial pressure support (Sellwood 1996).

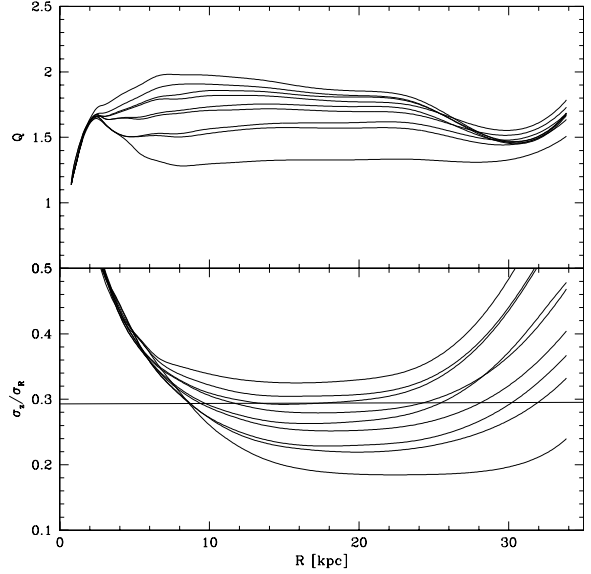


Fig. 2. The radial stability parameter Q (top) and the ratio σ_z/σ_R (bottom) as a function of the galactic radius. In both graphics, the curves correspond, from bottom to top, in the interval 10–20, to the models of increasing thickness, 01, 02, 07, 03, 08, 04, 09, 05, 06, respectively.

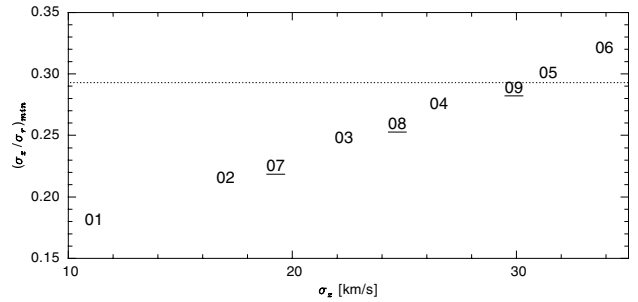


Fig. 3. Ratio σ_z/σ_R as a function of the vertical dispersion σ_z at $R = 15$ kpc. The values are taken at the radius where σ_z/σ_R is minimal. The dotted line corresponds to Araki's limit.

Table 1. Parameters R_f and h_{z0} for the different models. The respective flattening ζ of the total potential is also indicated.

Models	01	02	03	04	05	06
R_f	40	40	40	40	40	40
h_{z0}	0.05	0.15	0.25	0.35	0.45	0.55
$(\sigma_z/\sigma_R)_{\min}$	0.186	0.218	0.248	0.272	0.295	0.314
ζ	0.645	0.648	0.651	0.654	0.658	0.661
Models	07	08	09			
R_f	30	30	30			
h_{z0}	0.15	0.25	0.35			
$(\sigma_z/\sigma_R)_{\min}$	0.226	0.258	0.286			
ζ	0.648	0.652	0.656			

The models are evolved with the Barnes-Hut treecode parallelized to run on GRAVITOR, the 132-processor Beowulf cluster of the Geneva Observatory. To trust thin disk transverse instabilities it is important to not use an anisotropic Poisson

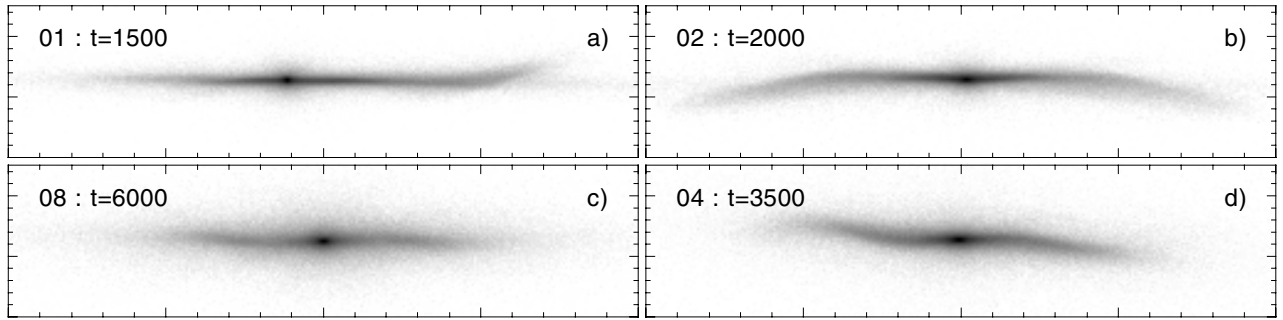


Fig. 4. Edge-on projections of the models 01, 02, 08, and 04. Times are indicated at the upper left. The box dimensions are $100 \times 25 \text{ kpc}^2$.

solver such as a polar grid mesh, therefore, despite being much more CPU time consuming, a treecode approach is preferred. Each simulation contains $2^{18} = 262\,144$ particles of equal mass. The softening length is 0.15 kpc, and the time-step is 0.5 Myr. If not indicated, the length unit is the kpc, and the time unit is the Myr.

3.2. Results

As expected, the evolution of the models depends strongly on the thickness of the heavy disk. In Fig. 3, from left to right, models can be divided in four groups:

- 1) Model 01 has a ratio σ_z/σ_R of 0.18. It is very unstable. The bending instability occurs quickly and generates a transient asymmetric warp that extends up to $z = 4 \text{ kpc}$ at $R = 35 \text{ kpc}$ (see Fig. 4a). The warp is associated with a spiral arm and its lifetime is about 1.5 Gyr. The ratio σ_z/σ_R is increased by the instability above Araki's limit, at about 0.4. After $t = 3000$, σ_z/σ_R is higher than 0.3 and the disk remains vertically stable. Face-on and edge-on projections of the model are displayed in Fig. 5.
- 2) Models 02, 07 and 03 have still a ratio σ_z/σ_R well below the Araki limit. The bending instability occurs during the first 2 Gyr. An axisymmetric bowl mode ($m = 0$) grows during about 1 Gyr, before that σ_z increases and stabilizes the disk. Figure 4b shows a spectacular U-shape warp of model 02 at $t = 2000$. During the instability, a large bulge forms, prolonged by a bar. The galaxies look like SBa types (see Fig. 5, $t > 2200 \text{ Myr}$). In model 07, the mode is slightly less symmetric, due to the lopsidedness of the galaxy. A short-lived $m = 1$ mode is present at the end of the instability, during the bar formation.
- 3) The four models 08, 04, 09 and 05 develop S-shaped warped modes ($m = 1$). Except for model 05 which has a ratio $\sigma_z/\sigma_R = 0.3$ just above Araki's limit, all are unstable with respect to bending. In the case of model 08, the warp is long-lived and lasts more than 5.5 Gyr, corresponding to about 5 rotation times at $R = 30 \text{ kpc}$ (see Fig. 6). In order to follow the evolution of the warped disk, we have divided it in a set of 18 concentric rings from $R = 0$ to 35 kpc . The inclination of each ring (warp angle) is determined by the direction of the major axis of the inertia tensor of the matter contained in the range $[R - \Delta R, R + \Delta R]$, where $\Delta R = 1 \text{ kpc}$ is the half width of the ring. The evolution

of the warp is displayed in Fig. 7 in form of Tip-LON diagrams (Briggs 1990). The diagrams represent the precession and nutation angle of each ring relative to the inner galactic disk. The outer dotted circle corresponds to an inclination of 3° . At $t = 500$, the disk is flat. The warp grows from $t = 1000$ to $t = 3000$ where it culminates ($z = 2 \text{ kpc}$ at $R = 35 \text{ kpc}$). During the following 4 Gyr, the amplitude of the warp slowly decreases. At $t = 6000$ it is still clearly observable (see Fig. 4c). Despite the differential rotation of the disk, the line of nodes (LON) remains quasi straight. However, in the outer parts, it is slightly trailing, contradicting Briggs' third rule (Briggs 1990)². The rotation period of the LON is about 1.1 Gyr, which corresponds to the circular rotation period at the edge of the disk ($R = 35 \text{ kpc}$). At about $t = 6500 \text{ Myr}$, the warp disappears and gives place to a large bar. The instability increases the vertical velocity dispersions by a factor 2 at the maximum, around 10 kpc. At larger radius, the factor is 1.5 or less. Velocities in the plane are unaffected. At the top of Fig. 8, we compare the warp angle of the four models at the time where the warp is maximum. The warp amplitude of model 04 is the highest. At $t = 3500$ it reaches more than 2 kpc above the plane defined by the central regions (see Fig. 4d). However, its lifetime is slightly shorter than model 02 and the warp disappears after 3.5 Gyr at $t = 5000$ (see the bottom of Fig. 8). The slightly thicker model 09 and 05 also develop warps with similar amplitudes but their lifetimes are shorter than 2.5 Gyr. In all four models, the warp shape is characterized by an inner flat region that extends between 5 to 10 kpc (Fig. 8, top).

- 4) Model 06 has a ratio σ_z/σ_R well above 0.3. In this model, no vertical instability occurs and the disk remains flat all along the simulation.

4. The influence of a dark halo

The previous simulations have been run in the absence of a dark halo, which has the advantage of allowing us to identify the warp origin uniquely to the self-gravity of the disk when Araki's instability criterion is met. We want now to check up to which point the disk self-gravity leads to bending instabilities when the disk is embedded in a conventional hot halo.

Since the bending instability is closely related to Araki's criterion, we determine how the threshold is modified by

² The galactic rotation is counterclockwise.

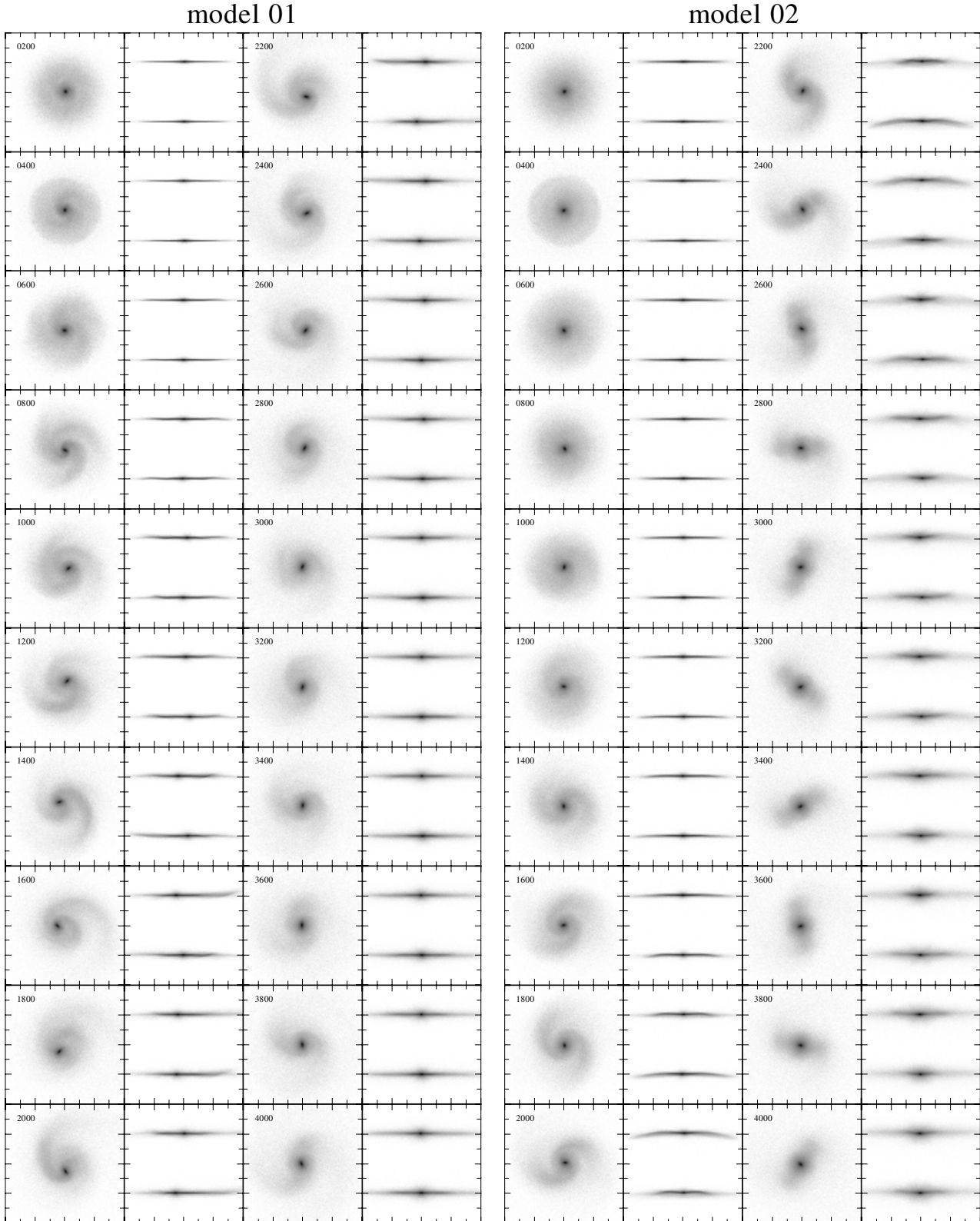


Fig. 5. Evolution of model 01 and 02 between $t = 200$ and $t = 4000$, noted in the upper left corner. Columns 1 to 4 show the face-on and two edge-on (perpendicular) projections of model 01, Cols. 5 to 8 correspond to model 02. The boxes dimensions are $50 \times 50 \text{ kpc}^2$.

different flattenings and mass of a hot dark halo. We suppose a hot halo because these are less subject to their own instabilities. Thus, a rigid potential is a convenient approximation of

the halo role, provided the velocity dispersions σ_z , σ_R in the disk are calculated consistently for the new local potential.

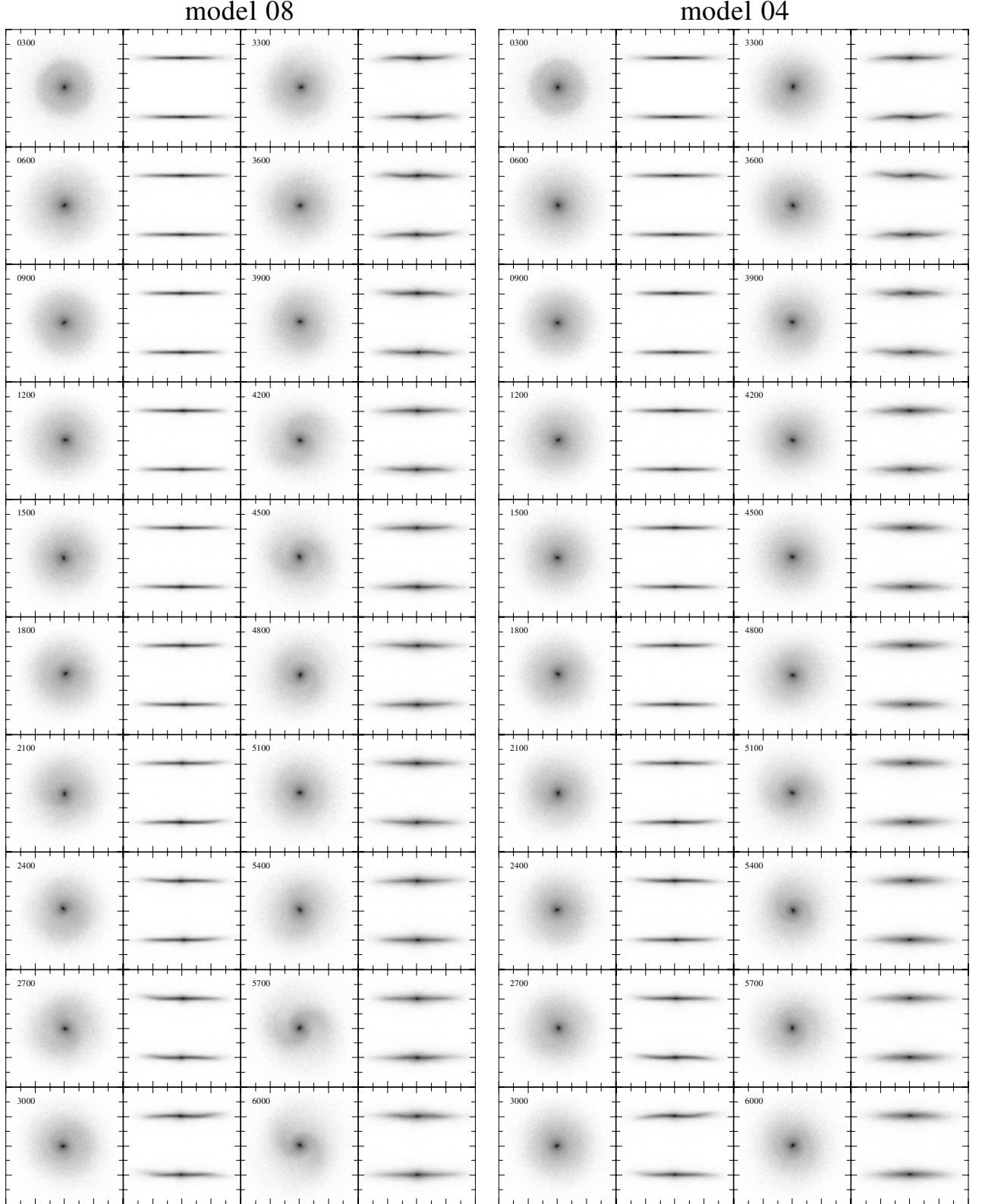


Fig. 6. Evolution of model 08 and 04 between $t = 300$ and $t = 6000$. Columns 1 to 4 show the face-on and two edge-on (perpendicular) projections of model 08, Cols. 5 to 8 correspond to model 04. The boxes dimensions are $50 \times 50 \text{ kpc}^2$.

4.1. Models with dark halos

The models with dark halos are based on the six first models with $R_f = 40 \text{ kpc}$. We simply add a quasi homogeneous thick

mass distribution in the disk region, however bounded in extension more abruptly than isothermal halos because we want to transfer mass from the heavy disk to the halo region of similar extent. Therefore we just adopt an inflated Plummer

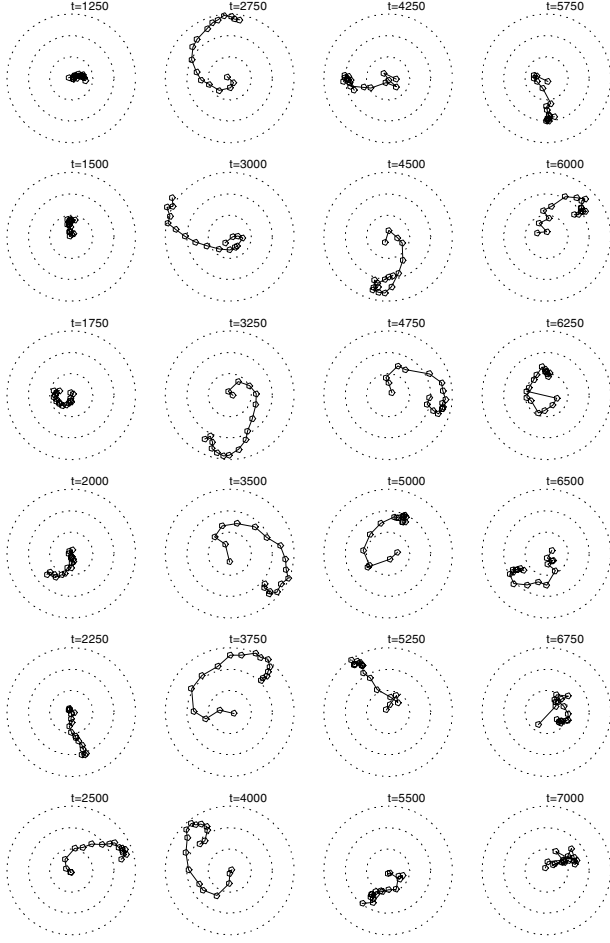


Fig. 7. Evolution of the warp in model 08 from $t = 1250$ to $t = 7000$ Myr. The diagrams show the polar angles of the rings (tip-LON plots). The three dotted circles mark $\theta = 1, 2, 3^\circ$.

potential, the Miyamoto-Nagai potential (Miyamoto & Nagai 1975) with a radial scale-length H of 20 kpc:

$$\phi_h = - \frac{GM_h}{\sqrt{R^2 + (H - c + \sqrt{z^2 + c^2})^2}}, \quad (8)$$

where c is the vertical scale-height. Here the constants in the potential are expressed differently from the original Miyamoto-Nagai potential in order to better express the horizontal scale length with H . The halo flattening is parametrized by $\zeta_h = c/H$. For $R < H$, ζ_h is a very good approximation of the ratio of minor over major axis of the mass iso-densities.

The mass fraction of dark matter that lies in the disk is parametrized by the factor f . We can thus write:

$$M_{hd} = f M_{\text{dark}}, \quad M_h = (1 - f) M_{\text{dark}} \quad (9)$$

where $M_{\text{dark}} = M_{hd} + M_h$. The total mass is then:

$$M_{\text{tot}} = M_b + M_d + f M_{\text{dark}} + (1 - f) M_{\text{dark}}. \quad (10)$$

4.2. Stability criterion

In the previous section, we have shown that the Araki limit is a good stability criterion against bending oscillations if it is applied to the minimum ratio σ_z/σ_R along the galactic radius.

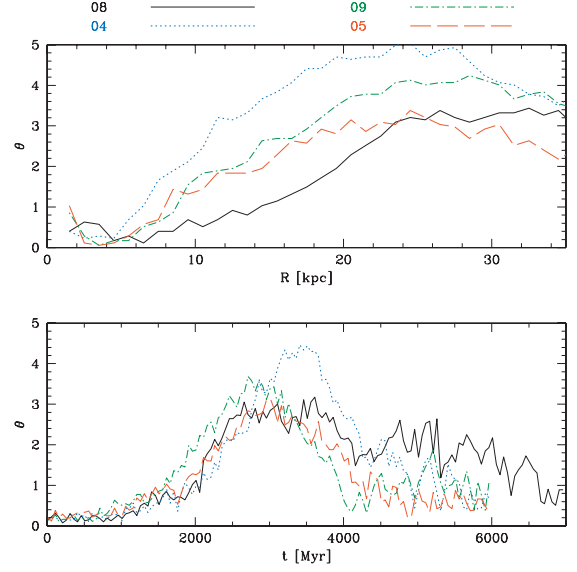


Fig. 8. *Top:* warp angle θ , as a function of radius, for the models 08 ($t = 3100$), 04 ($t = 3500$), 09 ($t = 2700$), and 05 ($t = 2800$). *Bottom:* time evolution of the mean warp angle computed between $R = 25$ and $R = 35$ kpc.

Since κ^2 and ν^2 are linear with respect to the mass, we can write (cf. Eq. (7)):

$$\frac{\sigma_z^2}{\sigma_R^2} = \beta^2 \frac{M_b \kappa_b^2 + M_d \kappa_d^2 + M_{\text{dark}} [f \kappa_{hd}^2 + (1 - f) \kappa_h^2]}{M_b \nu_b^2 + M_d \nu_d^2 + M_{\text{dark}} [f \nu_{hd}^2 + (1 - f) \nu_h^2]}, \quad (11)$$

where the ν_i and κ_i for each components are computed for a unit mass component. For the bulge, the exponential disk and the heavy disk, those values are obtained numerically with the Particle-Mesh potential solver. For the halo, these frequencies are calculated analytically.

For each of the 6 models, the influence of the dark matter fraction distributed in the disk or in the halo as well as the halo flattening is explored by varying the parameters f and ζ_h in the range 0 to 1. The results are plotted in Fig. 9. The Araki limit of 0.293 is traced with the solid bold line. The models that may be subject to bending instabilities ($\frac{\sigma_R}{\sigma_z} < 0.293$) are located at the bottom right of this line. On the contrary, stable models ($\frac{\sigma_R}{\sigma_z} > 0.293$) are located at the upper left.

In the absence of the halo ($f = 1$), results corresponds to the previous section. Models 01 to 04 are unstable and model 06 is stable. Model 05 is slightly above the Araki limit. However, as already mentioned, it develops a weak instability.

When the heavy disk is replaced by a spherical halo of equal mass ($f = 0$), the potential is smoothed around the $z = 0$ plane and the vertical epicycle frequency ν decreases. As κ is weakly modified, the ratio $\frac{\sigma_R}{\sigma_z}$ increases. Figure 9 shows that the model is stable as long as ζ_h is greater than 0.06. If $\zeta_h < 0.06$, the halo plays the role of the disk, and allows the bending instability to develop. It is relevant to note that between $\zeta_h = 0.5$ and 1, the halo flattening has little effect on the stability. If we consider dark halos with $\zeta_h \geq 0.5$, which corresponds to more realistic halos according to cosmological simulations (Dubinski & Carlberg 1991) and weak lensing studies (Hoekstra et al. 2004), the maximal halo mass in the

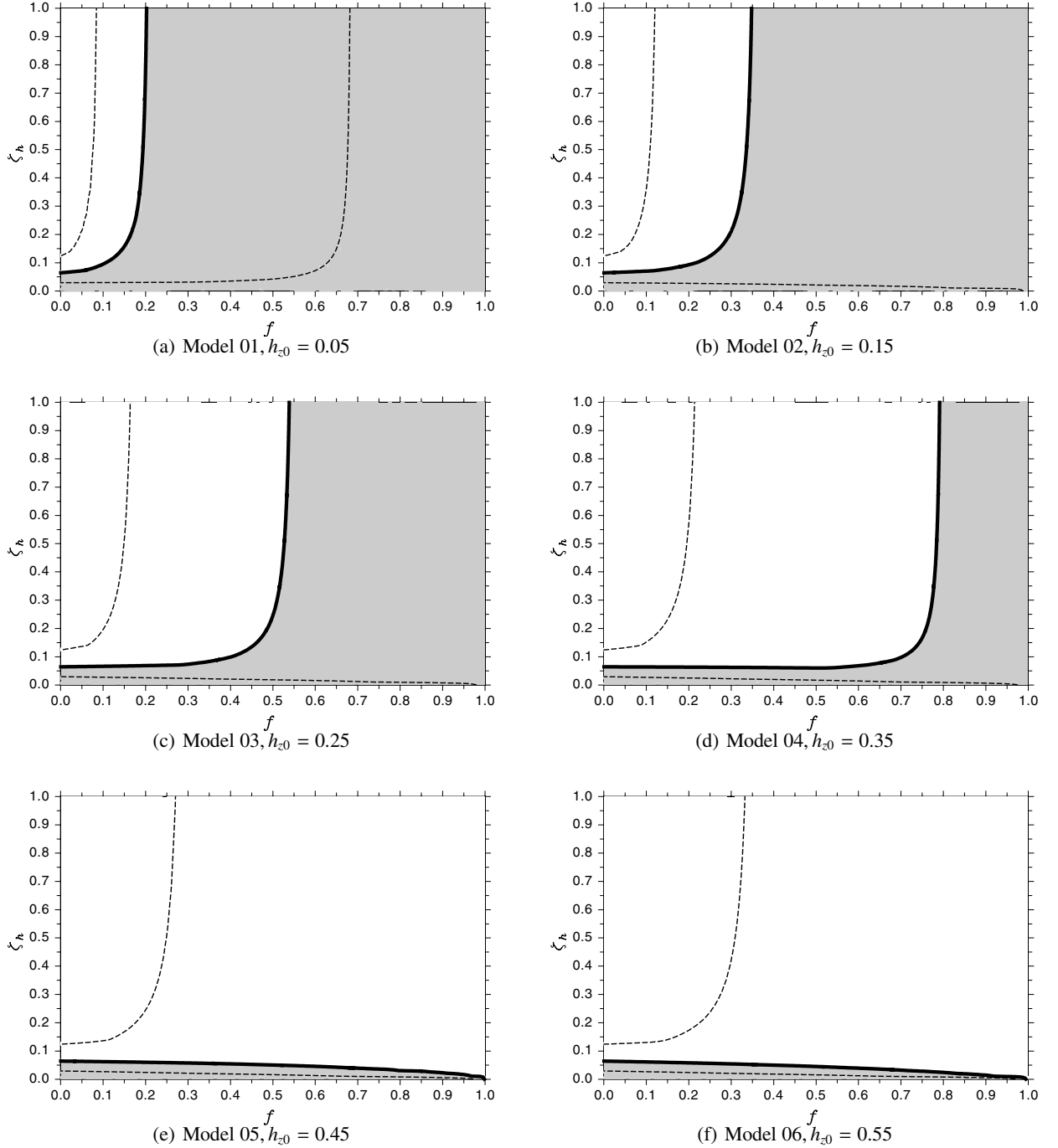


Fig. 9. Stability of the models with dark halos against the bending oscillations. The value of the minimum of $\frac{\sigma_R}{\sigma_z}$ along the radius, is plotted as a function of the fraction of dark matter in the heavy disk f and of the halo flattening ζ_h . The solid line corresponds to the critical value of 0.293. The upper dashed line corresponds to the values of 0.4 while bottom dashed line corresponds to 0.2. Shaded regions correspond to unstable models.

flatter disk case ($h_{z0} = 0.05$) must not be heavier than $0.8 M_{\text{dark}} (=0.58 M_{\text{tot}})$. For thicker disks, only a halo with a mass comparable to the heavy disk or less ($M_h \leq 0.36 M_{\text{tot}}$) allows bending instabilities to develop.

Some of our galaxy models can be used as first order representations of the Milky Way. If we assume that the Milky Way warp results from a bending instability and that the disk is most probably critical with respect to Araki's criterion, the

solid lines in Fig. 9 allow us to fix an approximate constraint on the halo to disk mass ratio. With a vertical scale-height of about 320 pc at the solar radius ($R_\odot = 8.5$ kpc), model 03 has a similar thickness to the Milky Way HI (Burton 1992). For any dark halo axis ratio larger than 0.3, the marginal stability of the disk implies a dark halo to heavy disk mass ratio around 1 (Fig. 9c). With this ratio, the surface density ($|z| < 700$ pc) of each component in units of M_\odot/pc^2 are: $\Sigma_b = 0.4$, $\Sigma_d = 36.7$,

$\Sigma_{\text{hd}} = 48.0$, $\Sigma_{\text{h}} = 3.7$, for a total surface density of $\Sigma_{\text{tot}} = 88.8$. The corresponding rotation velocity at the solar radius is 205 km s^{-1} .

5. Discussion

In this work, the vertical stability of a galaxy model where a substantial fraction of the gravitational matter is contained in the disk has been explored, leading to several aspects discussed below.

5.1. Bending instability vs. disk thickness

The strength of the investigated scenario is to require only intrinsic gravitational dynamics, therefore the reported effects are immediately produced whenever the stability threshold is reached, independently of spurious external torques produced by strong accretion events, galaxy interactions, a misaligned dark halo, or magnetic fields. In all the examined cases a sufficiently thin and massive disk produces a bending instability leading to a warp.

Our results were already expected by Merritt & Sellwood (1994) and Sellwood & Merritt (1994) in studies of counter-rotating disks, that $m = 0$ and $m = 1$ bending modes survive in disks without counter-rotation. Extremely thin disks with $h_{z0} < 150 \text{ pc}$ (potential flattening $\zeta < 0.648$) are strongly unstable and generate asymmetric transient warps, while thick disks with $h_{z0} \geq 550 \text{ pc}$ ($\zeta \geq 0.661$, $\sigma_z/\sigma_R \geq 0.3$) are completely stable. In between, $m = 0$ (U-shaped warp) and $m = 1$ (S-shaped warp) modes are excited. $m = 0$ modes grow for about 1 Gyr and disappear when the ratio σ_z/σ_R exceeds 0.3. S-shaped warps appear for thicker disks ($h_{z0} = 250\text{--}450 \text{ pc}$, $\zeta = 0.652\text{--}0.658$). They are characterized by a flat central disk and persistent straight LON, slightly trailing at large radius. The LON rotates at the circular velocity period of the disk edge. The most interesting result is that in model 08, the warp is persistent during 5.5 Gyr, a substantial fraction of the galaxy life. It is not clear if this persistent mode may be akin to the flapping mode reported by Sellwood (1996) in axisymmetric disks.

In our simulations, the two extreme disks (models 01 and 06) differ in their density thickness by a factor of 11. This translates to a potential flattening variation of only 2.5%. It is striking that observed galaxies have typical HI disk thickness in the range where bending instabilities can be triggered, because this transverse critical state would be similar to the disk radial state, which is also critical with respect to spiral arm formation.

Indeed, in more realistic models taking into account the dissipational behavior of the gas, energy dissipation reduces the gas velocity dispersion, and gaseous disks can be expected to reach a regime marginally unstable with respect to bending instabilities. This is similar to the bar and spiral instabilities in the plane which heat radially a weakly dissipative disk to a marginal stability $Q \sim 1\text{--}2$ state. Thus, we must expect that in more realistic models including gas dissipation, bending instabilities will be repeatedly excited.

Thus, a unifying picture of galactic disks emerges as dissipative systems maintained for a long time in a marginal stability state, where the effects of energy dissipation are

counter-balanced by dynamical instabilities in both the radial and vertical directions. Obviously star formation must also play an important role in compensating energy dissipation.

5.2. Comparison with observed warps

This idea of connecting gas dissipation to warps is supported by observations. Warps are more frequent among late type galaxies (Bosma 1991) and they are completely absent among lenticulars characterized by gas deficiency (Sánchez-Saavedra et al. 2003).

It is also noteworthy that the present scenario predicts a predominant occurrence of S-shaped warps, because in a slowly flattening disk due to energy dissipation, after the Araki instability threshold is crossed the S-shaped warps occur before the U-shaped ones.

As seen previously, only warps with modest amplitude are spontaneously generated, with warp angle less than 5° . Extreme cases, like for example NGC4013 (Bottema et al. 1987), which has a 25° warp angle, seem to require stronger causes than an internal instability, such as tidal interactions. However, as the warp angle distribution in optical surveys peaks at 3° (Reshetnikov 1998), this scenario may contribute to a large fraction of the S-shaped, the U-shaped, as well as the asymmetric warps observed in the optical.

5.3. Relationship between warps and dark halos

The semi-analytic analysis in Sect. 4 confirms our expectation that bending instabilities can occur as long as the self-gravity of the disk is locally dominant. If we accept that most galactic disks are thin and warped by bending instabilities, we obtain an additional constraint on the mass fraction and thickness of a dark spheroidal halo. For extreme thin disks, such as model 02, the halo mass fraction with respect to the *total* mass (using Fig. 9 and Eq. (10)) cannot exceed 0.47, for any halo flattening larger than ~ 0.3 . For more typical disk thicknesses, such as in model 03, the maximum halo mass fraction drops to 0.33, for any halo flattening larger than ~ 0.3 . The only way to obtain “classical” halos with a mass fraction of 0.9 is to decrease the halo flattening well below 0.1.

It is interesting to note that if now we assume that the warps are produced by an almost marginal instability state, the above halo mass fraction limits become equalities for any flattening above ~ 0.3 . Therefore the warps provide a sharp constraint on the halo relative mass, but a weak one on the halo flattening when the latter is above ~ 0.3 .

These results corroborate the recent independent study of Tyurina et al. (2004) where the halo mass of observed edge-on galaxies is estimated from the thickening of the disk due to the bending instabilities.

6. Conclusion

The most important result of this study is that long-lived galactic warps of observed amplitudes can be produced by internal bending instabilities, and that the dark matter to the total mass fraction within the warp radius and included in an extended

hot halo of similar extent is limited to about a factor of 2 if warps result from a marginal bending instability. Recent studies linking the spiral arms and kinematic properties of disk galaxies and the Milky-Way converge towards similar low values for dark halo masses within the HI disk range (Fuchs 2003; Kalberla 2003; Masset & Bureau 2003).

Further simulations combining a heavy disk and a live dark halo including dissipative gas or star formation feedback will allow us to specify in more detail these first order dynamical effects.

Acknowledgements. This work has been supported by the Swiss National Science Foundation. We thank Roger Fux for interesting discussions.

References

- Araki, S. 1985, Ph.D. Thesis, Massachusetts Inst. Technology
- Battaner, E., Florido, E., & Sánchez-Saavedra, M. L. 1990, *A&A*, 236, 1
- Binney, J. 1992, *ARA&A*, 30, 51
- Binney, J., & Tremaine, S. 1987, *Galactic Dynamic* (Princeton Univ. Press)
- Bissantz, N., Englmaier, P., & Gerhard, O. 2003, *MNRAS*, 340, 949
- Bosma, A. 1978, Ph.D. Thesis, Univ. Groningen
- Bosma, A. 1981, *AJ*, 86, 1825
- Bosma, A. 1981, *AJ*, 86, 1791
- Bosma, A. 1991, in *Warped disks and inclined rings around galaxies*, ed. S. Casertano, P. Sackett, & F. H. Briggs (Cambridge University Press)
- Bottema, R., Shostak, G. S., & van der Kruit, P. C. 1987, *Nature*, 328, 401
- Briggs, F. H. 1990, *ApJ*, 352, 15
- Broeils, A. 1992, Ph.D. Thesis, Rijksuniversiteit, Groningen
- Bureau, M., Freeman, K. C., Pfizner, W., & Meurer, G. R. 1999, *AJ*, 118, 2158
- Burke, B. F. 1957, *Astron. J.*, 62, 90
- Burton, W. B. 1992, in *The Galactic Interstellar Medium, Saas-Fee Advanced Course 21*, ed. D. Pfenniger, & P. Bartholdi, Berlin
- Carignan, C., Charbonneau, F., Boulanger, F., & Viallefond, F. 1990, *A&A*, 234, 43
- Cuillandre, J.-C., Lequeux, J., Allen, R. J., Mellier, Y., & Bertin, E. 2001, *ApJ*, 554, 190
- Dubinski, J., & Carlberg, R. G. 1991, *ApJ*, 378, 496
- Dubinski, J., & Kuijken, K. 1995, *ApJ*, 442, 492
- Fridman, A. M., & Polyachenko, V. L. 1984, *Physics of Gravitating Systems*, 2 (New York: Springer)
- Fuchs, B. 2003, *Astroph. Space Sci.*, 284, 719
- García-Ruiz, I., Kuijken, K., & Dubinski, K. 1998, in *Galactic Halos: A UC Santa Cruz Workshop*, ed. D. Zaritsky, ASP Conf. Ser., 136, 385
- Hernquist, L. 1991, in *Warped disks and inclined rings around galaxies*, ed. S. Casertano, P. Sackett, & F. H. Briggs (Cambridge University Press)
- Hoekstra, H., van Albada, T. S., & Sancisi, R. 2001, *MNRAS*, 323, 453
- Hoekstra, H., Yee, H. K. C., & Gladders, M. D. 2004, *ApJ*, 606, 67
- Huang, S., & Carlberg, R. G. 1997, *ApJ*, 480, 503
- Hunter, C., & Toomre, A. 1969, *ApJ*, 155, 747
- Jiang, I.-G., & Binney, J. 1999, *MNRAS*, 303, L7
- Kahn, F. D., & Woltjer, L. 1959, *ApJ*, 130, 705
- Kalberla, P. M. W. 2003, *ApJ*, 588, 805
- Kalnajs, A. 1999, in *The Third Stromlo Symposium: The Galactic Halo*, ed. B. K. Gibson, T. S. Axelrod, & M. E. Putman, ASP Conf. Ser., 165, 325
- Kerr, F. J., Hindman, J. V., & Carpenter, M. S. 1956, *Astron. J.*, 61, 8
- López-Corredoira, M., Betancort-Rijo, J., & Beckman, J. E. 2002, *A&A*, 386, 169
- Lynden-Bell, D. 1965, *MNRAS*, 129, 299
- Merritt, D., & Sellwood, J. A. 1994, *ApJ*, 425, 551
- Naeslund, M., & Joersaeter, S. 1997, *A&A*, 325, 915
- Masset, F. D., & Bureau, M. 2003, *ApJ*, 586, 152
- Miyamoto, M., & Nagai, R. 1975, *PASJ*, 27, 533
- Nelson, R. W., & Tremaine, S. 1995, *MNRAS*, 275, 897
- Newton, K., & Emerson, D. T. 1977, *MNRAS*, 181, 573
- Pfenniger, D., & Combes, F. 1994, *A&A*, 285, 91
- Pfenniger, D., & Friedli, D. 1993, *A&A*, 270, 561
- Pfenniger, D., Combes, F., & Martinet, L. 1994, *A&A*, 285, 79
- Quinn, T. 1991, *Nature*, 349, 571
- Reshetnikov, V., & Combes, F. 1998, *A&A*, 337, 9
- Reshetnikov, V., & Combes, F. 1999, *A&AS*, 138, 101
- Revaz, Y., & Pfenniger, D. 2001, in *Gas and Galaxy Evolution*, ed. J. E. Hibbard, M. Rupen, & J. H. van Gorkom, San Francisco, ASP Conf. Proc., 240, 278
- Richter, O. G., & Sancisi, R. 1994, *A&A*, 290, L9
- Roberts, M. S. 1966, *ApJ*, 144, 639
- Rogstad, D. H., Wright, M. C. H., & Lockhart, I. A. 1976, *ApJ*, 204, 703
- Sánchez-Saavedra, M. L., Battaner, E., & Florido, E. 1990, *MNRAS*, 246, 458
- Sánchez-Saavedra, M. L., Battaner, E., Guizarro, A., et al. 2003, *A&A*, 399, 457
- Sancisi, R. 1976, *A&A*, 53, 159
- Sellwood, J. A. 1996, *ApJ*, 473, 733
- Sellwood, J. A., & Merritt, D. 1994, *ApJ*, 425, 530
- Smith, D. A., Allen, R. J., Bohlin, R. C., Nicholson, N., & Stecher, T. P. 2000, *ApJ*, 538, 608
- Sparke, L. S. 1984, *MNRAS*, 211, 911
- Sparke, L., & Casertano, S. 1988, *MNRAS*, 234, 873
- Toomre, A. 1966, *Geophys. Fluid Dyn.*, 46, 111
- Tyurina, N. V., Khoperskov, A. V., & Bizyaev, D. 2004, preprint [arXiv:astro-ph/0405142]
- Weiner, B. J., Sellwood, J. A., & Williams, T. B. 2001, *ApJ*, 546, 931